Rayleigh instability of charged aggregates: Role of the dimensionality, ionic strength, and dielectric contrast

M. N. Tamashiro
Max-Planck-Institut für Polymerforschung, Ackermannweg 10, 55128 Mainz, Germany;
Instituto de Física, Universidade de São Paulo, Caixa Postal 66318, 05315-970 São Paulo, São Paulo, Brazil;
and Instituto de Física Gleb Wataghin, Universidade Estadual de Campinas, Caixa Postal 6165, 13083-970 São Paulo, Campinas, Brazil

H. Schiessel
Max-Planck-Institut für Polymerforschung, Ackermannweg 10, 55128 Mainz, Germany
and Instituut-Lorentz, Universiteit Leiden, P. O. Box 9506, 2300 JA Leiden, The Netherlands
(Received 28 July 2005; revised manuscript received 11 July 2006; published 28 August 2006)

We extended a previous analysis of the classical Rayleigh instability of spherical charged droplets in the presence of neutralizing monovalent counterions [M. Deserno, Eur. Phys. J. E **6**, 163 (2001)], by generalizing the problem for suspensions of aggregates with D-dimensional symmetry, corresponding for $D=2$ to infinite (rodlike) cylindrical charged bundles and for $D=3$ to spherical charged droplets. In addition, we include the effects of added monovalent salt and of dielectric contrast between the charged aggregate and the surrounding solvent. The electrostatic energy taking the microion screening into account is estimated using uniform profiles within the framework of the cell model. We verify the robustness of these results by also considering Debye-Hückel-type microion profiles that are obtained by the minimization of a linearized Poisson-Boltzmann free-energy functional. In the case when the microions can enter inside the charged aggregates, we confirm the occurrence of a discontinuous phase change between aggregates of finite size and an infinite aggregate, which takes place at a collapse temperature that depends on their volume fraction ϕ and on the salt content. Decrease of ϕ shifts the phase-change temperature toward higher values, while salt addition has an opposite effect. We obtain analytical expressions for the phase-separation line in the asymptotic limit of infinite dilution ($\phi \to 0$), showing that the collapse temperature depends logarithmically on ϕ. As an application for $D=3$ we discuss the stability of the pearl-necklace structures of flexible polyelectrolytes in poor solvents. The case $D=2$ is applied to the problem of finite bundle sizes of stiff polyelectrolytes that attract each other—via, e.g., multivalent counterions—leading to an effective surface tension.

DOI: 10.1103/PhysRevE.74.021412 PACS number(s): 82.70.−y, 36.40.Qv, 68.03.Cd, 05.70.−a

I. INTRODUCTION

More than one century after the pioneering work of Lord Rayleigh on the instability of charged droplets [1], there is still room for investigations on the subject [2,3]. The classical Rayleigh instability arises from the competition between the bulk electrostatic repulsion and the interfacial surface tension. Increasing the size or the charge density of a spherical droplet leads to capillary instabilities that eventually split up the droplet into smaller ones, each carrying charges below the instability threshold. Especially in the field of charged soft matter the Rayleigh instability has recently became popular as a possible mechanism underlying the formation of finite-sized charged aggregates. One example is the formation of pearl-necklace structures for flexible polyelectrolytes (charged polymers) in poor solvents—where the collapsed liquidlike polymer droplet is broken up into smaller-sized spherical pearls connected via strings [4]—and that of polyampholytes (polymers carrying positive and negatively charged monomers)—where also necklaces with multidisperse-sized pearls appear [5,6]. In a similar spirit, but for a different symmetry, it has been recently suggested [7] that the Rayleigh instability might also be responsible for the experimentally observed finite size of bundles (cylindrical aggregates) of rodlike stiff polyelectrolytes like double-stranded DNA [8], F-actin [9], and microtubules [10]. This theory—predicting thermodynamically stable finite bundles—has to be contrasted with previous ones which suggest that kinetic effects lead to finite aggregation sizes [11–14].

At a more abstract level all these systems can be considered as an emulsion of a charged liquid, the polymer solute (dispersed phase), in a polarizable liquid, the surrounding solvent (continuous phase), these two liquids being immiscible. The surface tension between these liquids arises from the effective attraction between the monomers comprising the polymer, which results from the hydrophobicity of the polyelectrolyte [4], the Debye-Hückel-type attraction between the monomers in the polyampholyte [5], or the multivalent counterion-induced attraction between the rods [15–21], respectively.

What distinguishes these soft-matter applications from the classical Rayleigh instability is the presence of neutralizing counterions in the solution and—usually—that of salt ions. Furthermore, dielectric contrast between the charged aggregate and the surrounding solvent usually plays a role. This leads to several questions. Does counterion condensation onto the finite-sized charged aggregate destroy the Rayleigh mechanism, as a result leading to a stable infinite aggregate?—as, e.g., was suggested on the basis of scaling arguments in Refs. [22–26]. What happens if the aggregate is impenetrable to the microions due to excluded volume or

dielectric contrast? What is the role of the volume fraction of the charged aggregate for the Rayleigh mechanism? Does the presence of salt prevent or enhance the Rayleigh instability? How does the dimensionality (spherical versus cylindrical aggregates) enter into the physics of the Rayleigh instability?

Two recent papers have addressed some of these questions. Deserno [27] has considered two immiscible liquids (the charged solute and the polarizable solvent) in the absence of salt, but in the presence of neutralizing monovalent counterions; see also a similar simplified analysis applied for colloidal cluster phases and the problem of gelation [28]. He assumed that there is a microphase separation between the two liquids, the charged fluid forming spherical droplets immersed in the surrounding solvent. Two cases were analyzed: (a) the charged droplets are impenetrable to the counterions and (b) the counterions can enter inside the charged droplets. He found that the Rayleigh droplets are always stable in the first case, but become unstable in the latter, once a sufficient fraction of counterions has condensed inside the charged droplets (due to an increase of the electrostatic coupling strength). This fraction of condensed counterions that induces macroscopic phase separation decreases with a decrease of the volume fraction ϕ of the charged fluid, so that for a sufficiently small value of ϕ the droplets coalesce as soon as counterion condensation sets in. A recent paper by Henle and Pincus [7] put forward a similar mechanism to explain the finite bundle size of rodlike polyelectrolytes that attract each other via, e.g., the presence of monovalent coions and mono- and multivalent counterions. Assuming that only the multivalent counterions can enter the aggregate, it was found that the bundles grow to infinite thickness once a sufficient amount of multivalent counterions is present. If, however, there is in addition a steric cost for the counterions to enter the aggregate, the bundle is stabilized at a finite thickness.

The purpose of the present study is to present a unified view of the Rayleigh instability in charged aggregates with two- (cylindrical) and three-dimensional (spherical) symmetries in the presence of monovalent counterions, added monovalent salt and dielectric contrast between the aggregate and the solvent. In Sec. II we extend the model proposed by Deserno [27] to include all these effects. Our results are presented in Sec. III and Sec. IV discusses their possible applications. The Appendix contains the asymptotic forms of the phase-separation parameters in the infinite-dilution ($\phi \to 0$) limit. The interested reader may find several nontrivial derivations and technical details in Appendixes A-F, which are presented in the form of an associated EPAPS document [29].

II. DEFINITION OF THE MODEL

The general theoretical framework is described in detail in Ref. [27] for a suspension of spherical charged droplets in the presence of neutralizing monovalent counterions only. We recall here the important definitions and also present the generalizations introduced. Without loss of generality, we will consider polyanionic (negatively charged) aggregates (in three dimensions) that have a D-dimensional symmetry—for example, $D=2$ for infinite (rodlike) cylindrical charged bundles and $D=3$ for spherical charged droplets. The bare volumetric charge density $-q\rho$ of the aggregates, treated as an incompressible fluid, occupies a volume fraction ϕ of the suspension and has a surface tension $k_BT\gamma$ with respect to the surrounding solvent [30], where we introduced the proton elementary charge q and the thermal energy $k_BT \equiv \beta^{-1}$. The aggregates have a cross-section radius a and are located at the center of a Wigner-Seitz cell of radius $R=a\phi^{-1/D}$ (see Fig. 1). To measure the strength of the electrostatic interactions inside the solvent, considered as a linear and isotropic continuum of dielectric constant $\epsilon_>$, we define the Bjerrum length $l_B=\beta q^2/\epsilon_>$ which corresponds to the distance at which the electrostatic interaction energy of two elementary charges immersed in the solvent equals the thermal energy. For water at room temperature $l_B=7.15$ Å. The aggregates will also be treated as a linear and isotropic medium of dielectric constant $\epsilon_<=\epsilon_>\epsilon$. It will be convenient to introduce the dimensionless distances

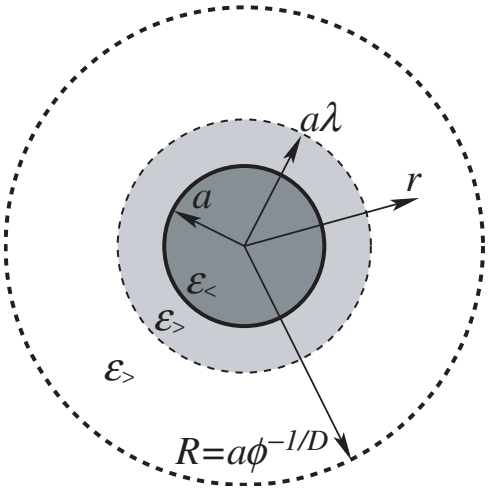

FIG. 1. Two-dimensional representation of a Wigner-Seitz cell of radius $R=a\phi^{-1/D}$ containing a charged aggregate in its center (represented by the dark gray region) of cross-section radius a and dielectric constant $\epsilon_<=\epsilon_>\epsilon$, where $\epsilon_>$ is the dielectric constant of the solvent in the region $r>a$. For $D=2$ the cell is cylindrical with an infinite length—the geometry shown corresponds to a cross section perpendicular to the symmetry axis. For $D=3$ the cell has a spherical symmetry and the figure represents a cross section at a plane containing the center of the cell. Therefore, the generalized radial coordinate r corresponds to the radial distance from the symmetry axis for $D=2$ and to the distance to the center of the cell for $D=3$. We will assume the existence of a condensed layer of microions within the intermediate shell $a<r<a\lambda$ (represented by the light gray region).

$$\tilde{l}_B = l_B\gamma^2/\rho \quad \text{and} \quad \tilde{a} = a\rho/\gamma. \tag{1}$$

The analysis performed in Ref. [27] is restricted only to screening due to neutralizing counterions released by the charged aggregate, which ensure the overall charge neutrality of the system. In our extended study, addition of monovalent salt to the suspension is parametrized by the intensive ratio between the number of ionized pairs of salt particles N_s and

the number of neutralizing monovalent counterions N_c, both per cell,

$$s \equiv \frac{N_s}{N_c}. \tag{2}$$

Therefore, the calculations are performed in the canonical ensemble, in order to avoid the explicit investigation of the Donnan-equilibrium problem [31–34], when the suspension is in electrochemical equilibrium through a semipermeable membrane with an infinite reservoir of fixed bulk salt density. This study is required to express the effective salinity of the suspension s in terms of the salinity of the salt reservoir s_{res} (cf. Ref. [34]).

The microion profiles are treated at the level of a three-zone Oosawa model [35], i.e., they are taken as uniform and are classified according to three regions: inside the charged aggregate, within a condensed layer, and free (unbounded). We assume that fractions α'_+ of the cations (including the positive counterions) and α'_- of the anions (coions) can enter inside the charged aggregates in the region $0<r<a$. A fraction α_+ of the cations and a fraction α_- of the anions are free (located at the outermost shell $a\lambda<r<R$), while the remaining microions are inside a condensed layer in the intermediate shell $a<r<a\lambda$ (with $\lambda>1$).

We introduce the linear combinations

$$\alpha'(\alpha'_\pm) = (1+s)\alpha'_+ - s\alpha'_-, \tag{3}$$

$$\alpha(\alpha_\pm) = (1+s)\alpha_+ - s\alpha_-, \tag{4}$$

$$\nu'(\alpha'_\pm) = (1+s)\alpha'_+ + s\alpha'_-, \tag{5}$$

related to the effective charge of microions inside the aggregate, to the effective charge of free microions, and to the total fraction of microions that enter inside the aggregate, respectively. Although we formulate the problem such that the microions can enter inside the charged aggregates, i.e., such that they are permeable ("soft") to the microions, the case of impenetrable ("hard") aggregates can be obtained by taking appropriate limits of the penetrable case, namely, by enforcing $\alpha'_+=\alpha'_-=0$.

The Helmholtz free-energy density f (per charged monomer of the aggregate [36], in unities of k_BT) may then be written as

$$\frac{\beta f}{\rho\phi} = \frac{2\pi}{D}\tilde{l}_B\tilde{a}^2 U_D(\alpha',\alpha,\lambda) + S_D(\alpha'_\pm,\alpha_\pm,\lambda) + \frac{D}{\tilde{a}} + S_{ideal} + \nu'(\alpha'_\pm)\beta\Delta u. \tag{6}$$

The functions U_D and S_D are related to the electrostatic energy and the mixing entropy of the system, respectively, while the third term $D/\tilde{a}$ is associated with the surface-tension energy. Because uniform profiles for the microions were assumed, it is straightforward to obtain U_D and S_D by integration of the Poisson equation (using Gauss's law) and assuming that the mobile microions behave like ideal gases. Their explicit expressions, as well as the ideal-gas entropy S_{ideal} of the microions, are given in Appendix A [29]. Finally, the last term arises from the difference of the solvation energy Δu of the microions due to the dielectric contrast (cf. Appendix B [29]). This contribution, estimated by the Born equation [37,38]

$$\beta\Delta u = (\epsilon^{-1}-1)\frac{l_B}{2r_0}, \tag{7}$$

is obtained assuming that the microions are hard spheres of radius $r_0 \ll a$ carrying elementary charges $\pm q$ distributed uniformly on their surfaces, whose dielectric constant is the same as the medium in which they are embedded—$\epsilon_<$ inside and $\epsilon_>$ outside the aggregate, respectively.

Some particular cases can be obtained by taking appropriate limits of Eq. (6).

(a) By imposing $\alpha'_+=\alpha'_-=0$ from the beginning we regain the case when the microions remain outside the charged aggregate. For a salt-free suspension of spherical charged droplets in the absence of dielectric contrast ($s\to 0$, $D=3$, $\epsilon=1$) this corresponds to the case 1 treated in Ref. [27].

(b) By taking $s\to 0$, $D=3$, and $\epsilon=1$ we regain the results of Ref. [27] for a salt-free suspension of spherical charged droplets in the absence of dielectric contrast: case 2, ions can penetrate the droplet.

(c) In the absence of a condensed layer we have automatically $\alpha'_\pm=1-\alpha_\pm$ and $\lambda\to 1$. For $D=3$ this does not affect qualitatively the results obtained with a condensed layer (Sec. III A), while for $D=2$ there is a profound difference between the two treatments (Sec. III B).

For a given reduced Bjerrum length $\tilde{l}_B$, volume fraction ϕ, and salt content s, the equilibrium size of the aggregate is found by minimization of the free-energy density Eq. (6) with respect to $\tilde{a}$,

$$4\pi\tilde{l}_B\tilde{a}^3 = \frac{D^2}{U_D(\alpha',\alpha,\lambda)}. \tag{8}$$

Although minimization with respect to the five remaining variables $(\alpha'_\pm,\alpha_\pm,\lambda)$ can always be numerically performed, it will be convenient to obtain the stationary-point conditions $\delta(f/\rho\phi)=0$ in analytical form,

$$\begin{pmatrix} 1+s & 0 & 0 \\ 0 & 1+s & 0 \\ 0 & 0 & 1 \end{pmatrix} \cdot \hat{\nabla} U_D(\alpha',\alpha,\lambda) = -\left(\frac{2U_D^2}{\pi\tilde{l}_B D}\right)^{1/3}\left[\hat{\nabla}_+ S_D(\alpha'_\pm,\alpha_\pm,\lambda) + \beta\Delta u\begin{pmatrix} 1+s \\ 0 \\ 0 \end{pmatrix}\right], \tag{9}$$

where the differential operators

$$\hat{\nabla} \equiv \begin{pmatrix} \partial/\partial\alpha' \\ \partial/\partial\alpha \\ \partial/\partial\lambda \end{pmatrix}, \quad \hat{\nabla}_+ \equiv \begin{pmatrix} \partial/\partial\alpha'_+ \\ \partial/\partial\alpha_+ \\ \partial/\partial\lambda \end{pmatrix}$$

and the anion-associated variables (α'_-,α_-) at equilibrium can be written explicitly in terms of the cation-associated variables (α'_+,α_+) (see Appendix C [29]). For the particular cases where $\alpha'_\pm$ are constrained to a subspace—for example, cases (a) and (c) of the preceding paragraph—the first row of

Eq. (9) is not present and the coupled system has to be solved for two variables only (α_+ and λ).

For the general case when the microions are allowed to enter inside the aggregates, there is a minimum associated with the Helmholtz free-energy density of the aggregate of infinite size,

$$\frac{\beta \bar{f}_\beta}{\rho\phi} = \bar{S}_\beta + \bar{\nu}'_\beta \beta\Delta u + S_{\text{ideal}}, \tag{10}$$

where the subscript β emphasizes the temperature dependence of the associated functions through the ionic solvation-energy difference (in unities of k_BT) $\beta\Delta u$. The mixing entropy $\bar{S}_\beta$ and the parameter $\bar{\nu}'_\beta$, both associated with the aggregate of infinite size, are given in Appendix D [29]. However, for sufficiently small values of $\tilde{l}_B$ the aggregate of infinite size is metastable, that is, its associated Helmholtz free-energy density, given by Eq. (10), is higher than that corresponding to the aggregate of finite size, defined by Eqs. (6)–(9). For fixed values of ϕ and s, there is a unique set of parameters $(\alpha'^*_\pm, \alpha^*_\pm, \lambda^*)$ for which the free-energy densities of the infinite and finite aggregates coincide, $\bar{f}_{\beta^*} = f(\alpha'^*_\pm, \alpha^*_\pm, \lambda^*)$, giving rise to a discontinuous phase change (see Fig. 3 of Ref. [27] for the special case $s \to 0$, $D=3$, and $\epsilon=1$). At this particular set of parameters there is a macroscopic phase separation of the dispersed (charged liquid) and the continuous (surrounding solvent) phases [39]. The phase-separation values of $\tilde{a}$ and $\tilde{l}_B$ [40],

$$\tilde{a}^* = \frac{3D}{2[\bar{S}_{\beta^*} - S_D(\alpha'^*_\pm, \alpha^*_\pm, \lambda^*) - (\nu'^* - \bar{\nu}'_{\beta^*})\beta^*\Delta u]}, \tag{11}$$

$$\tilde{l}_B^* = \frac{2[\bar{S}_{\beta^*} - S_D(\alpha'^*_\pm, \alpha^*_\pm, \lambda^*) - (\nu'^* - \bar{\nu}'_{\beta^*})\beta^*\Delta u]^3}{27\pi D U_D(\alpha'^*, \alpha^*, \lambda^*)}, \tag{12}$$

are given in terms of the phase-separation parameters $(\alpha'^*_+, \alpha^*_+, \lambda^*)$, which satisfy the coupled system of three equations

$$[\bar{S}_{\beta^*} - S_D(\alpha'^*_\pm, \alpha^*_\pm, \lambda^*) - (\nu'^* - \bar{\nu}'_{\beta^*})\beta^*\Delta u] \times \begin{pmatrix} 1+s & 0 & 0 \\ 0 & 1+s & 0 \\ 0 & 0 & 1 \end{pmatrix} \cdot \hat{\nabla} U_D(\alpha'^*, \alpha^*, \lambda^*) = -3U_D(\alpha'^*, \alpha^*, \lambda^*) \left[\hat{\nabla}_+ S_D(\alpha'^*_\pm, \alpha^*_\pm, \lambda^*) + \beta^*\Delta u \begin{pmatrix} 1+s \\ 0 \\ 0 \end{pmatrix} \right], \tag{13}$$

where the phase-separation anion-associated variables $(\alpha'^*_-, \alpha^*_-)$ have the same form as the ones at equilibrium (given in Appendix C [29]) evaluated at the phase-separation parameters and $(\alpha'^*, \alpha^*, \nu'^*)$ are also given by Eqs. (3)–(5), replacing $(\alpha'_\pm, \alpha_\pm)$ by their phase-separation values $(\alpha'^*_\pm, \alpha^*_\pm)$.

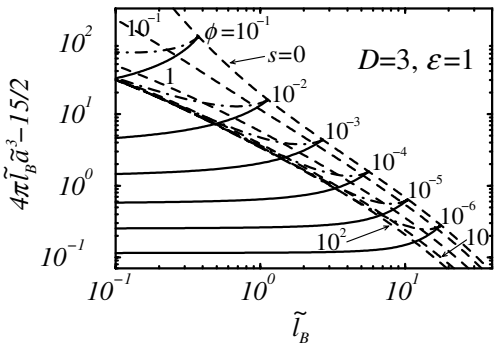

FIG. 2. Phase-separation cross-section radius $\tilde{a}^*$ as a function of $\tilde{l}_B$ for aggregates of spherical symmetry ($D=3$) in the absence of dielectric contrast ($\epsilon=1$) and several values of s and ϕ. Dashed lines are obtained for constant amount of salt (varying from $s=0$ to 100, from right to left), while dot-dashed lines are obtained for constant volume fraction (varying from $\phi=10^{-1}$ to 10^{-6}, from top to bottom). Note the existence of a lower bound for the phase-separation line as the salt concentration (measured by the parameter s) increases. The solid lines correspond to the equilibrium-size salt-free curves ($s=0$) for fixed values of ϕ, and terminate at the salt-free phase-separation dashed line. For values of ϕ below the critical value $\phi^{\text{crit}}=4.413\ldots\times10^{-5}$ the equilibrium-size salt-free curves are in fact discontinuous functions of $\tilde{l}_B$ (see magnification in Fig. 3). The details shown in Fig. 3, especially the gray coexistence region, could not be seen if they would be plotted here in unmagnified scale.

III. RESULTS

A. Spherical droplets ($D=3$) in the absence of dielectric contrast ($\epsilon=1$)

The salt-free case ($s=0$) was analyzed in Ref. [27] where it was shown that the equilibrium droplet radius is always larger than the classical Rayleigh instability value, $4\pi\tilde{l}_B\tilde{a}^3 > 15/2$. In Fig. 2 we show the salt-free equilibrium droplet radius as a function of $\tilde{l}_B$ for several values of the volume fraction ϕ. These curves terminate at a phase-separation line where the system undergoes a discontinuous collapse phase change. Along this line droplets of finite radius coalesce into a single infinite droplet, leading to macroscopic phase separation. In Fig. 2 we also show the effect of addition of monovalent salt to the phase-separation line. For a fixed temperature $\tilde{l}_B$, there is a lower bound for this line as the salt concentration (measured by the parameter s) increases.

In the Appendix we give analytical expressions for the asymptotic behavior of the phase-separation parameters in the infinite-dilution limit ($\phi \to 0$). We should remark that the uniform-profile model always predicts the existence of a condensed layer of counterions. Even in the infinite-dilution limit, there is a fraction $1-\alpha'^*_+-\alpha^*_+=0.028\,145\cdots+O(\phi\ln\phi)$ of condensed counterions. This may be somewhat misleading, since the thickness of the condensation layer diverges, $\lambda^*=\phi^{-1/3}0.304\,18\cdots+O(\ln\phi)$, leading to the equality of the concentrations of the condensed and free counterions. Therefore, in this limit, we cannot distinguish condensed from free counterions and this would, in fact, cor-

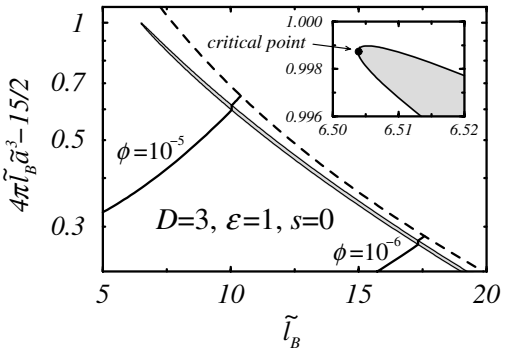

FIG. 3. Magnification of the salt-free ($s=0$) phase-separation droplet radius $\tilde{a}^*$ as a function of $\tilde{l}_B$ (dashed line) for aggregates of spherical symmetry ($D=3$) in the absence of dielectric contrast ($\epsilon=1$). The solid lines correspond to the equilibrium-size salt-free curves for two small values of ϕ, showing that they are in fact discontinuous functions of $\tilde{l}_B$. In the gray region distinct thermodynamic phases, characterized by finite droplets with two different radii, may coexist. In the inset we show this region in the vicinity of the critical point (black dot), located at $(\tilde{l}_B^{\text{crit}}, \log_{10}\phi^{\text{crit}})=(6.503\ldots,-4.355\ldots)$. For volume fractions below this critical value, $\phi<\phi^{\text{crit}}$, besides the macroscopic phase separation that occurs at lower temperatures (dashed line), there is a discontinuous phase change associated with this two-phase coexistence. We emphasize that this magnification corresponds to a subtle detail of Fig. 2—note the scales of the axes. The banana-shaped phase coexistence region is very narrow and it is not presented in Fig. 2, since it would not be possible to identify it on the unmagnified scale of Fig. 2.

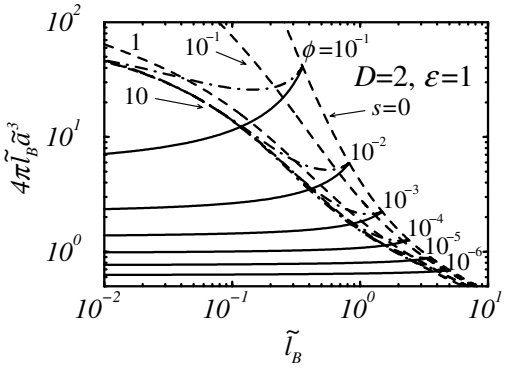

FIG. 4. Phase-separation cross-section radius $\tilde{a}^*$ as a function of $\tilde{l}_B$ for aggregates of cylindrical symmetry ($D=2$) in the absence of dielectric contrast ($\epsilon=1$) and several values of s and ϕ. Dashed lines are obtained for constant amount of salt (varying from $s=0$ to 10, from right to left), while dot-dashed lines are obtained for constant volume fraction (varying from $\phi=10^{-1}$ to 10^{-6}, from top to bottom). As in the case of spherical aggregates, the position of the phase-separation line reaches a saturation value as the salt concentration increases. Note, however, that the phase-separation line in the infinite-dilution limit has no lower bound, $\lim_{\phi\to 0}4\pi\tilde{l}_B^*\tilde{a}^{*3}\to 0$. On this scale, the position of the phase-separation line for $s=100$ is indistinguishable from the one for $s=10$. The solid lines correspond to the equilibrium-size salt-free curves ($s=0$).

respond to a counterion release (or evaporation). For the salt-free system ($s=0$), the asymptotic phase-separation temperature reads $\tilde{l}_B^*=\frac{5}{243\pi}|\ln\phi|^3[1+O(\phi^{1/3}\ln\phi)]$. This asymptotic analytical result should be compared with the numerical fitting (for ϕ in the range $10^{-4}\leqslant\phi\leqslant 1$) found by Deserno [27], $\tilde{l}_B^*(\phi)\approx 0.13|\ln\phi|+0.0056|\ln\phi|^3$.

An interesting point is the existence of a discontinuous phase change between phases associated to finite droplets with two different radii. In Fig. 3 we show, for the salt-free system ($s=0$), the narrow coexistence region associated with this discontinuous phase change, which terminates at a critical point in analogy with first-order transitions in macroscopic systems. This phase change and its associated critical behavior, however, are artifacts of the uniform-profile model: as shown in Appendix E [29], they disappear by inclusion of nonuniform Debye-Hückel-type counterion profiles for the outer region. These profiles are obtained within a linearized Poisson-Boltzmann approximation [41–44]. A similar simpler analysis was applied for the transition from small to big charged unilamellar vesicles [45]; see also Ref. [46] for the nonlinear treatment of this transition.

B. Cylindrical bundles ($D=2$) in the absence of dielectric contrast ($\epsilon=1$)

The system behavior presented in Fig. 4 is similar to the spherical case, with the existence of a lower bound (at a fixed temperature $\tilde{l}_B$) for the phase-separation line as the salt concentration increases. However, contrary to the spherical case—which is limited by the classical Rayleigh instability value $4\pi\tilde{l}_B^*\tilde{a}^{*3}=15/2$—there is no lower bound for the phase-separation line in the cylindrical case as the temperature decreases, $\lim_{\tilde{l}_B\to\infty}4\pi\tilde{l}_B^*\tilde{a}^{*3}\to 0$. It is noteworthy, however, that the phase-equilibrium Manning parameter in the infinite-dilution limit, $\lim_{\phi\to 0}\xi^*=\pi\tilde{l}_B^*\tilde{a}^{*2}=2/3$ (see Fig. 5), coincides with the threshold Manning parameter, found in Ref. [20], for the unbinding transition (or the onset of rod-rod attrac-

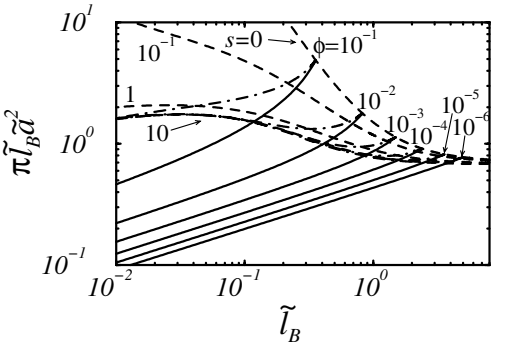

FIG. 5. Same as in Fig. 4, but using the Manning parameter $\xi\equiv\pi\tilde{l}_B\tilde{a}^2$ as variable for the y axis. The solid lines correspond to the salt-free ($s=0$) equilibrium Manning parameter curves, while the dashed and dot-dashed lines correspond to the phase-separation Manning parameter with varying salt content s and volume fraction ϕ, respectively. Note that the infinite-dilution limit of the phase-separation Manning parameter does not vanish, $\lim_{\phi\to 0}\xi^*=\pi\tilde{l}_B^*\tilde{a}^{*2}=2/3$.

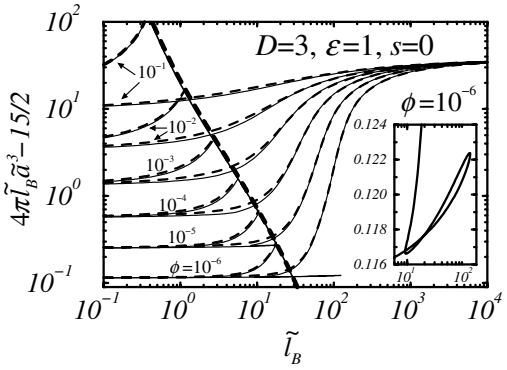

FIG. 6. Comparison of the salt-free ($s=0$) droplet equilibrium radius as a function of $\tilde{l}_B$ for aggregates of spherical symmetry ($D=3$) in the absence of dielectric contrast ($\epsilon=1$) for decreasing volume fractions, varying from $\phi=10^{-1}$ to 10^{-6} (from top to bottom). Solid lines are obtained with the uniform-profile model [27], and dashed lines with the linearized Poisson-Boltzmann profiles for the outer region derived in Appendix E [29]. Except for the spurious discontinuous phase change between two phases associated with finite droplets with different radii (see also Fig. 3) the uniform-profile model describes well the main features of the system. The inset shows the unstable branch of the droplet equilibrium radius for the lowest volume fraction, $\phi=10^{-6}$. Curves extending to the right (at lower temperatures) are obtained when the counterions cannot enter inside the droplets, while the curves terminating at a phase-separation line (represented by the thick diagonal curves) are obtained when the counterions are allowed to enter inside the droplets. At this phase-separation value, droplets of finite radius would coalesce into a single droplet of infinite size, leading to macroscopic phase separation.

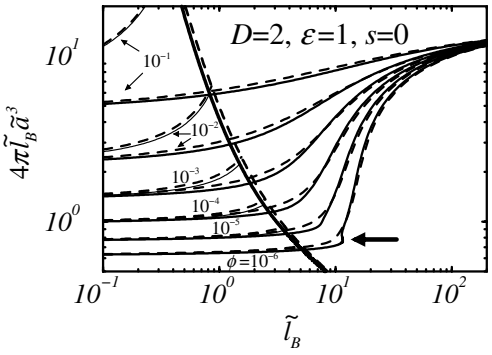

FIG. 7. Comparison of the salt-free ($s=0$) equilibrium cross-section radius as a function of $\tilde{l}_B$ for aggregates of cylindrical symmetry ($D=2$) in the absence of dielectric contrast ($\epsilon=1$) for decreasing volume fractions, varying from $\phi=10^{-1}$ to 10^{-6} (from top to bottom). The meaning of the curves is the same as in Fig. 6. The uniform-profile model still yields a spurious discontinuous phase change for very dilute systems, but the effect is less pronounced than in the spherical case. Note the narrow unstable branch of the equilibrium cross-section radius for the lowest volume fraction, $\phi=10^{-6}$, denoted by the large arrow.

tion) between two like-charged rods in the regime of large coupling parameters, whose value is smaller than the Manning counterion-condensation threshold for a single rod, $\xi=1$ [47].

In the Appendix we give analytical expressions for the asymptotic behavior of the phase-separation parameters in the infinite-dilution limit ($\phi\to 0$), which are explicitly derived in Appendix F [29]. It is shown that their behavior is distinct from the asymptotics obtained for a system without the condensed layer of microions. Therefore, for the cylindrical symmetry it is essential to include a condensed layer of microions to describe correctly the system, because this layer is still present even in the infinite-dilution limit. For a salt-free system, this behavior is analogous to the Manning counterion condensation [47,48] for rodlike polyelectrolytes.

C. Salt-free ($s=0$) impenetrable aggregates in the absence of dielectric contrast ($\epsilon=1$)

Deserno showed in his study [27] that the Rayleigh droplets are stable for any given value of $\tilde{l}_B$ when the counterions cannot enter the droplets (cf. Fig. 2 of Ref. [27]). In that case the equilibrium droplet size has the asymptotic behavior $4\pi\tilde{l}_B\tilde{a}^3\to 45$ in the low-temperature limit $\tilde{l}_B\to\infty$, independently of the volume fraction ϕ. We reproduced this result in Fig. 6 where we also compare it with the curves obtained with a Debye-Hückel-type profile in the outer region, which have the same low-temperature asymptotics. Similar behavior is also found in the case of cylindrical symmetry depicted in Fig. 7. Enforcing that the counterions stay outside the cylindrical aggregates, their equilibrium thickness approach the limit $4\pi\tilde{l}_B\tilde{a}^3\to 16$ as the temperature vanishes ($\tilde{l}_B\to\infty$), independently of the volume fraction ϕ. However, in both cases (cylindrical and spherical symmetries), the uniform-profile model predicts, at low volume fractions, a spurious discontinuous phase change between phases associated with finite aggregates with two different cross-section radii (see Figs. 6 and 7). These artifacts are eliminated by using the nonuniform Debye-Hückel-type profiles in the outer region, derived in Appendix E [29].

D. Effect of dielectric contrast ($\epsilon\neq 1$) on salt-free ($s=0$) cylindrical bundles ($D=2$)

Dielectric contrast may drastically alter the system behavior. An aggregate whose dielectric constant $\epsilon_<$ is very low may hinder the penetration of the microions, and the system would behave as in the case of an impenetrable aggregate. Of course, one should keep in mind that usually a low-dielectric bulk is not charged at all. However, a low-dielectric environment might still be capable of becoming charged if the corresponding counterions find a nearby high-dielectric medium that can host these ions, an idea put forward in Refs. [49,50]. In the case of reverse dielectric constrast, the ionic solvation may also depend on their polarizability and on the size of the high-dielectric aggregate [51].

In Fig. 8 we present the effect of dielectric contrast on the equilibrium cross-section radius and the phase-separation line of salt-free cylindrical aggregates. The solvation-energy difference was estimated using the Born equation (7) with a fixed ratio $l_B/r_0=2$. One can note two general trends upon ϵ

decreasing: (a) the equilibrium cross-section radius of the aggregate shrinks; (b) the phase-separation line moves toward higher $\tilde{l}_B$ values, associated with lower temperatures. The smaller equilibrium thickness of the aggregates reflects the fact that their electrostatic energies are higher than those corresponding to aggregates with the same thickness but in the absence of dielectric contrast ($\epsilon=1$). On the other hand, the shift of the phase-separation lines toward higher $\tilde{l}_B$ values can be understood by the fact that the counterions avoid entering into the aggregates due to the large solvation-energy cost originated from the dielectric contrast. The collapse of the aggregate is only possible at stronger electrostatic coupling, when the counterion condensation sets in.

It is noteworthy that the solvation energy is crucial for the stabilization of the low-dielectric aggregates. By just considering the mean-field electrostatic energy and neglecting the solvation energy, one might reach the conclusion that the dielectric reduction inside the charged aggregates would favor its neutralization by the intrusion of the counterions. However, inclusion of the Born energy hinders the penetration of the microions due to the high-energy cost. The net effect is determined by the relative magnitudes of these two antagonistic effects—the mean-field type, favoring neutralization, and the non-mean-field type, opposing the penetration of microions inside the aggregate.

IV. DISCUSSION AND CONCLUSION

The general outcome of this study is that the Rayleigh mechanism that leads to the formation of finite-size aggregates breaks down once enough counterions enter the aggregates upon, e.g., an increase in the electrostatic coupling, leading to macroscopic phase separation. This discontinuous phase change takes place at smaller values of $\tilde{l}_B$ (i.e., at higher temperatures) when the volume fraction and/or the salt concentration is higher (cf. Figs. 2 and 4). On the other hand, the Rayleigh aggregates are stable for all $\tilde{l}_B$ values if they are impenetrable to microions (cf. Figs. 6 and 7) since in this case macroscopic phase separation would lead to macroscopic charge separation. Dielectric contrast also has a pronounced effect on the size and stability of Rayleigh aggregates: the lower their dielectric constant the smaller their equilibrium radius (due to the electrostatic self-energy of the aggregate) and the wider the range of $\tilde{l}_B$ values where they are stable (due to the increased self-energy of ions inside the aggregate) (see Fig. 8). All this is valid both for spherical and cylindrical aggregates. The main difference between (spherical) droplets and (cylindrical) bundles is that in the former case the phase-equilibrium line has the classical Rayleigh instability value as a lower bound, $4\pi\tilde{l}_B^*\tilde{a}^{*3}\rightarrow 15/2$, whereas in the latter case no lower bound is found in the infinite-dilution ($\phi\rightarrow 0$) limit, $\lim_{\phi\rightarrow 0} 4\pi\tilde{l}_B^*\tilde{a}^{*3}=0$. We obtain, however, a nonvanishing phase-equilibrium Manning parameter in the infinite-dilution limit, $\lim_{\phi\rightarrow 0}\xi^*=\pi\tilde{l}_B^*\tilde{a}^{*2}=2/3$, whose numerical value coincides with the threshold Manning parameter for the unbinding transition between two like-charged rods in the regime of large coupling parameters [20].

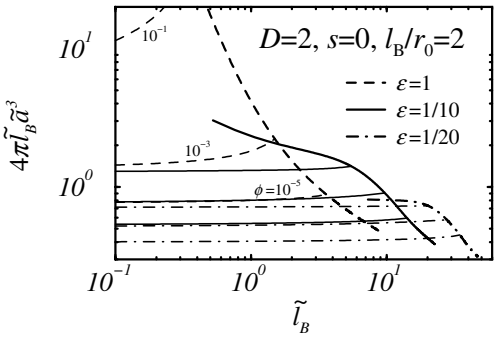

FIG. 8. Salt-free ($s=0$) equilibrium (thin lines) and phase-separation cross-section radii (thick diagonal curves) as a function of $\tilde{l}_B$ for aggregates of cylindrical symmetry ($D=2$) and decreasing volume fractions, varying from $\phi=10^{-1}$ to 10^{-5} (from top to bottom) for two different dielectric ratios $\epsilon=1/10$ (solid lines) and $1/20$ (dot-dashed lines). The solvation-energy difference was estimated using the Born equation (7) with a fixed ratio $l_B/r_0=2$. To allow a comparison with the results in the absence of dielectric contrast, we also presented the $\epsilon=1$ curves with penetration of the counterions inside the aggregates (dashed lines).

We speculate next about the role of the Rayleigh instability in the phase behavior of flexible polyelectrolytes. It is known that a flexible polyelectrolyte in a poor solvent may form a necklace [4]. This structure is a tradeoff between surface tension and electrostatic repulsion: a neutral polymer in a poor solvent prefers to form a spherical globule due to the surface tension, but the electrostatic repulsion between charged monomers in a polyelectrolyte leads to a breakup of this single globule into smaller-sized pearls due to the Rayleigh instability. The connectivity of the polymer is reflected in the fact that these pearls are connected via thin strings into a necklace configuration. The scaling theory for necklaces was developed, however, for the case when counterion condensation is absent [4]. This leads to the question whether necklaces might also be stable once counterion condensation sets in. Scaling studies [22–25] came to the conclusion that necklaces should not be stable with respect to counterion condensation and should collapse instead, the prediction being that the necklace collapses with the first counterion condensing. This was predicted for both counterions condensing on single spherical pearls—the phase boundary between states "6" and "9" in Ref. [24]—and for condensation on the whole necklace—the phase boundary between states "7" and "9" in Ref. [24]—at which boundary the necklace turns out to be cylindrical.

This result is of profound importance since many polyelectrolytes have water as the poor solvent *and* are beyond the counterion-condensation threshold, which might explain the difficulty in finding necklaces experimentally. At the same time, however, necklaces have been seen in computer simulations of flexible polyelectrolytes in poor-solvent conditions that were highly charged enough to show counterion condensation. These chains clearly showed necklaces with condensed counterions [52–55].

Of course, scaling arguments, as given in Refs. [22–25], are not capable of predicting the precise value at which a

necklace collapses, leaving the opportunity for a range of parameters where counterions could be condensed on a still stable necklace. In fact, the study by Deserno [27] was aiming at this fact and showed that there is indeed a parameter range at which stable Rayleigh droplets with a finite fraction of intruded counterions do exist. Similarly we showed the same behavior for cylindrical symmetry, which, as stated above, is also of relevance in understanding the case of counterion condensation on the necklace as a whole. In addition, we showed in the present study that the phase-separation fraction of intruded counterions at which the Rayleigh aggregate becomes unstable decreases with decreasing volume fraction according to expressions for $\alpha_+'^*$ giving in the Appendix for spherical and cylindrical symmetries, both showing a leading $\phi^{1/3}$ dependence of $\alpha_+'^*$ [56]. This indeed shows that at sufficiently small volume fractions it is the first counterion intruding into the aggregate that leads to the breakdown of the Rayleigh instability and the concomitant collapse of the chain. In that sense the scaling prediction of necklace collapse as soon as counterions condense onto beads or onto the whole necklace is indeed correct. The stability of necklaces seen in computer simulations even in the presence of counterions [52–55] might be explained by the finite range of stable structures at finite-chain concentrations or, more likely, by the stability of impenetrable droplets, since the solvent quality in these simulations is typically very poor, resulting in dense pearls.

Similarly for bundles, as put forward recently [7], the finite bundle size of charged rodlike chains might be explained by the space limitations for counterions inside the aggregate. This is especially likely for highly charged chains like double-stranded DNA, where a single molecule is already far above the counterion-condensation threshold. Our study shows that impenetrable bundles are always stable and that in presence of dielectric contrast the range at which bundles stay finite is considerably extended.

ACKNOWLEDGMENTS

The authors thank M. Deserno, C. Holm, K. Kremer, Y. Levin, H.-J. Limbach, and P. Pincus for helpful discussions. The authors acknowledge the financial support of the Max-Planck Gesellschaft and the Alexander von Humboldt-Stiftung, Germany. M.N.T. also thanks the financial support of Fapesp, Fundação de Amparo à Pesquisa do Estado de São Paulo, Brazil.

APPENDIX: ASYMPTOTIC BEHAVIOR OF THE PHASE-SEPARATION PARAMETERS IN THE INFINITE-DILUTION LIMIT

For spherical aggregates ($D=3$), the asymptotic phase-separation parameters in the infinite-dilution limit ($\phi\to 0$) are given by

$$\alpha_+'^* = a_0\phi^{1/3}(1+a_1\phi^{1/3}) + O(\phi\ln\phi),$$

$$\alpha_+^* = 1 - a_2^3 + O(\phi^{1/3}\ln\phi),$$

$$\lambda^{*3}\phi = a_2^3 + O(\phi^{1/3}\ln\phi),$$

$$\tilde{a}^* = \frac{9}{2}\left[\frac{3}{2}\ln a_0 - \ln\phi + (1+s)a_0\phi^{1/3}\left(1 - \ln a_0 + \frac{2}{3}\ln\phi\right)\right]^{-1} + O(\phi^{2/3}\ln\phi),$$

$$\tilde{l}_B^* = \frac{5}{243\pi}\left[\frac{3}{2}\ln a_0 - \ln\phi + \frac{1}{2}\phi^{1/3}\left(2(1+s)a_0 + \frac{3}{2}\ln a_0 - \ln\phi\right)\right]^3 + O(\phi^{2/3}\ln\phi),$$

$$4\pi\tilde{l}_B^*\tilde{a}^{*3} = \frac{15}{2}\left[1 + \left(\frac{3}{2} + 2(1+s)a_0\right)\phi^{1/3}\right] + O(\phi^{2/3}\ln\phi).$$

Note that the asymptotic behavior of the phase-separation parameters $\tilde{a}^*$ and $\tilde{l}_B^*$ for the leading and subleading orders depends only on the dominant prefactor of $\alpha_+'^*$, $a_0 = s^{2s/3}/(1+s)^{2(1+s)/3}$. The numerical value of the coefficient $a_2 = 0.304\,183\,47\ldots$, given by the real zero $\in[0,1]$ of the polynomial $4a_2^5+4a_2^4+4a_2^3-13a_2^2-13a_2+5$, is irrelevant for the two leading orders of the asymptotic phase-separation behavior. It should be remarked that a_0 and the subleading prefactor $a_1 = -\frac{1}{3}a_0\left[1-2s-(1+s)\ln a_0+\frac{2}{3}(1+s)\ln\phi\right]$ both coincide with the asymptotic prefactors obtained for a system *without* the condensed layer of microions. The physical reason for this coincidence for spherical symmetry is the spread of the microion cloud (microion evaporation) in the infinite-dilution limit.

For cylindrical aggregates ($D=2$), the asymptotic phase-separation parameters in the infinite-dilution limit ($\phi\to 0$) read

$$\alpha_+'^* = b_0\phi^{1/3} + O(\phi^{2/3}\ln\phi),$$

$$\alpha_+^* = 1 - b_1 + O(\phi^{1/3}\ln\phi),$$

$$\lambda^{*2}\phi = b_2 + O(\phi^{1/3}\ln\phi),$$

$$\tilde{a}^* = 3[s\ln s - (1+s)\ln(1+s) - \ln\phi + \Xi_1(b_1,b_2,s)]^{-1} + O(\phi^{1/3}\ln\phi),$$

$$\tilde{l}_B^* = -\frac{2}{27\pi}\frac{[s\ln s - (1+s)\ln(1+s) - \ln\phi + \Xi_1(b_1,b_2,s)]^3}{1+\ln\phi+\Xi_2(b_1,b_2,s)} + O(\phi^{1/3}\ln\phi),$$

$$\pi\tilde{l}_B^*\tilde{a}^{*3} = -2[1+\ln\phi+\Xi_2(b_1,b_2,s)]^{-1} + O(\phi^{1/3}\ln\phi).$$

The coefficients $\{b_j\}$—which depend on s and ϕ, cf. Eqs. (F5) and (F6)—and the functions $\{\Xi_j(b_1,b_2,s)\}$ are given in Appendix F [29].

[1] Lord Rayleigh, Philos. Mag. **14**, 184 (1882).

[2] I. Last, Y. Levy, and J. Jortner, Proc. Natl. Acad. Sci. U.S.A. **99**, 9107 (2002).

[3] D. Duft, H. Lebius, B. A. Huber, C. Guet, and T. Leisner, Phys. Rev. Lett. **89**, 084503 (2002); D. Duft, T. Achtzehn, R. Müller, B. A. Huber, and T. Leisner, Nature (London) **421**, 128 (2003).

[4] A. V. Dobrynin, M. Rubinstein, and S. P. Obukhov, Macromolecules **29**, 2974 (1996).

[5] Y. Kantor and M. Kardar, Phys. Rev. E **51**, 1299 (1995).

[6] V. Yamakov, A. Milchev, H.-J. Limbach, B. Dünweg, and R. Everaers, Phys. Rev. Lett. **85**, 4305 (2000).

[7] M. L. Henle and P. A. Pincus, Phys. Rev. E **71**, 060801(R) (2005).

[8] V. A. Bloomfield, Curr. Opin. Struct. Biol. **6**, 334 (1996); Biopolymers **44**, 269 (1997).

[9] T. E. Angelini, H. Liang, W. Wriggers, and G. C. L. Wong, Proc. Natl. Acad. Sci. U.S.A. **100**, 8634 (2003).

[10] D. J. Needleman, M. A. Ojeda-Lopez, U. Raviv, H. P. Miller, L. Wilson, and C. R. Safinya, Proc. Natl. Acad. Sci. U.S.A. **101**, 16099 (2004).

[11] B.-Y. Ha and A. J. Liu, Phys. Rev. Lett. **81**, 1011 (1998).

[12] B.-Y. Ha and A. J. Liu, Europhys. Lett. **46**, 624 (1999).

[13] J. F. Stilck, Y. Levin, and J. J. Arenzon, J. Stat. Phys. **106**, 287 (2002).

[14] Y. Levin, Rep. Prog. Phys. **65**, 1577 (2002).

[15] I. Rouzina and V. A. Bloomfield, J. Phys. Chem. **100**, 9977 (1996).

[16] N. Grønbech-Jensen, R. J. Mashl, R. F. Bruinsma, and W. M. Gelbart, Phys. Rev. Lett. **78**, 2477 (1997).

[17] B.-Y. Ha and A. J. Liu, Phys. Rev. Lett. **79**, 1289 (1997); **83**, 2681 (1999); Y. Levin, J. J. Arenzon, and J. F. Stilck, *ibid.* **83**, 2680 (1999).

[18] B. I. Shklovskii, Phys. Rev. Lett. **82**, 3268 (1999).

[19] M. Deserno, A. Arnold, and C. Holm, Macromolecules **36**, 249 (2003).

[20] A. Naji, A. Arnold, C. Holm, and R. R. Netz, Europhys. Lett. **67**, 130 (2004).

[21] H.-J. Limbach, M. Sayar, and C. Holm, J. Phys.: Condens. Matter **16**, S2135 (2004).

[22] H. Schiessel and P. Pincus, Macromolecules **31**, 7953 (1998).

[23] A. V. Dobrynin and M. Rubinstein, Macromolecules **32**, 915 (1999).

[24] H. Schiessel, Macromolecules **32**, 5673 (1999).

[25] T. A. Vilgis, A. Johner, and J.-F. Joanny, Eur. Phys. J. E **2**, 289 (2000).

[26] A. V. Dobrynin and M. Rubinstein, Macromolecules **34**, 1964 (2001).

[27] M. Deserno, Eur. Phys. J. E **6**, 163 (2001).

[28] J. Groenewold and W. K. Kegel, J. Phys.: Condens. Matter **16**, S4877 (2004).

[29] See EPAPS Document No. E-PLEEE8-74-204608 for the associated Appendixes A-F. For more information on EPAPS, see http://www.aip.org/pubservs/epaps.html.

[30] Although we will treat the bare charge density ρ and the surface tension γ as independent parameters, in general they have to be determined by the local short-ranged interactions and might depend on the temperature, ionic strength, etc. See, e. g., Y. Levin, J. Stat. Phys. **110**, 825 (2003), for a thermodynamic derivation of the ionic-strength dependence of the excess surface tension γ of a liquid-vapor interface in aqueous electrolyte solutions.

[31] F. G. Donnan, Chem. Rev. (Washington, D.C.) **1**, 73 (1924).

[32] J. Th. G. Overbeek, Prog. Biophys. Biophys. Chem. **6**, 57 (1956).

[33] V. Reus, L. Belloni, T. Zemb, N. Lutterbach, and H. Versmold, J. Phys. II **7**, 603 (1997).

[34] M. N. Tamashiro, Y. Levin, and M. C. Barbosa, Eur. Phys. J. B **1**, 337 (1998).

[35] F. Oosawa, J. Polym. Sci. **23**, 421 (1957); F. Oosawa, *Polyelectrolytes* (Marcel Dekker, New York, 1971).

[36] Even though the Helmholtz free-energy density per charged monomer $f/(\rho\phi)$ is not an intensive quantity in the number of charged monomers per cell $\rho\phi v$, where v is the volume of a Wigner-Seitz cell associated with a single aggregate, minimizing the Helmholtz free energy $F=fV$ of a suspension of fixed total volume V is equivalent to minimize $f/(\rho\phi)$ for incompressible aggregates (constant density ρ) occupying a fixed volume fraction ϕ of the suspension.

[37] M. Born, Z. Phys. **1**, 45 (1920).

[38] R. Messina, J. Chem. Phys. **117**, 11062 (2002).

[39] We should remark that we are not treating this macroscopic phase separation as a standard first-order phase transition, in which coexistence between macroscopic phases is determined by the equality of the intensive fields (pressure, temperature, and chemical potential). This phenomenon will be termed more properly a *discontinuous phase change* and is driven by the competition between the long-ranged electrostatic repulsion and the short-ranged surface tension. Both effects contribute nonextensively to the internal energy and one cannot apply the standard thermodynamics of macroscopic systems [H. B. Callen, *Thermodynamics and an Introduction to Thermostatistics*, 2nd ed. (John Wiley & Sons, New York, 1985)], but rather the "small-systems thermodynamics" [T. L. Hill, *Thermodynamics of Small Systems* (Dover, New York, 1994); *Statistical Mechanics* (McGraw-Hill, New York, 1956), Appendix 9]. In order to simplify the analysis and not enter into this delicate issue, we decided to consider that the phase change, which may be viewed as a nucleation process, takes place at the droplet radius for which the Helmholtz free energies of the finite-droplet and the infinite-droplet systems become equal. Viewed as a nucleation process, this collapse radius corresponds to the limit of stability below which clusters remain finite and above which clusters grow into macroscopic (infinite) droplets.

[40] In the presence of dielectric contrast ($\Delta u \neq 0$), because of the temperature dependence of the right-hand side of Eq. (12) (see Appendixes C and D [29], α'_-, α_-, $\bar{S}_\beta$ and $\bar{v}'_\beta$ depend on $\beta\Delta u$) this relation is in fact an additional transcendental equation for $\tilde{l}_B^*$, which has to be solved simultaneously with Eq. (13). In the absence of dielectric contrast ($\Delta u=0$), the right-hand side of Eq. (12) is, however, independent of the temperature and Eqs. (12) and (13) are decoupled.

[41] H. H. von Grünberg, R. van Roij, and G. Klein, Europhys. Lett. **55**, 580 (2001).

[42] M. Deserno and H. H. von Grünberg, Phys. Rev. E **66**, 011401 (2002).

[43] M. N. Tamashiro and H. Schiessel, J. Chem. Phys. **119**, 1855 (2003).

[44] M. N. Tamashiro and H. Schiessel, Phys. Rev. E **68**, 066106

(2003).
[45] J. Oberdisse, Eur. Phys. J. B **3**, 463 (1998).
[46] J. Oberdisse and G. Porte, Phys. Rev. E **56**, 1965 (1997).
[47] G. S. Manning, J. Chem. Phys. **51**, 924 (1969); Q. Rev. Biophys. **11**, 179 (1978); G. S. Manning and J. Ray, J. Biomol. Struct. Dyn. **16**, 461 (1998).
[48] E. Trizac and G. Téllez, Phys. Rev. Lett. **96**, 038302 (2006).
[49] A. Parsegian, Nature (London) **221**, 844 (1969).
[50] J. Schmit, R. Menes, and P. A. Pincus, Phys. Rev. E **66**, 061502 (2002).
[51] Y. Levin, Pramana, J. Phys. **64**, 957 (2005).
[52] U. Micka, C. Holm, and K. Kremer, Langmuir **15**, 4033 (1999).
[53] U. Micka and K. Kremer, Europhys. Lett. **49**, 189 (2000).
[54] H.-J. Limbach, C. Holm, and K. Kremer, Europhys. Lett. **60**, 566 (2002).
[55] H.-J. Limbach and C. Holm, J. Phys. Chem. B **107**, 8041 (2003).
[56] Note, however, that the prefactor b_0 for cylindrical symmetry, given by Eq. (F4), has a weak dependence on ln ϕ, see Appendix F [29].